JACS
JOURNAL OF THE AMERICAN CHEMICAL SOCIETY

ARTICLE

pubs.acs.org/JACS

Engineering Encodable Lanthanide-Binding Tags into Loop Regions of Proteins

Katja Barthelmes,[†] Anne M. Reynolds,[‡] Ezra Peisach,[§] Hendrik R. A. Jonker,[†] Nicholas J. DeNunzio,[§] Karen N. Allen,[*,§] Barbara Imperiali,[*,‡] and Harald Schwalbe[†,*]

[†]Institute for Organic Chemistry and Chemical Biology, Center for Biomolecular Magnetic Resonance, Johann Wolfgang Goethe-University of Frankfurt, Max-von-Laue-Strasse 7, 60438 Frankfurt, Germany

[‡]Departments of Chemistry and Biology, Massachusetts Institute of Technology, 77 Massachusetts Avenue, Cambridge, Massachusetts 02139, United States

[§]Department of Chemistry, Boston University, 590 Commonwealth Avenue, Boston, Massachusetts 02215, United States

Supporting Information

ABSTRACT: Lanthanide-binding tags (LBTs) are valuable tools for investigation of protein structure, function, and dynamics by NMR spectroscopy, X-ray crystallography, and luminescence studies. We have inserted LBTs into three different loop positions (denoted L, R, and S) of the model protein interleukin-1β (IL1β) and varied the length of the spacer between the LBT and the protein (denoted 1−3). Luminescence studies demonstrate that all nine constructs bind Tb^{3+} tightly in the low nanomolar range. No significant change in the fusion protein occurs from insertion of the LBT, as shown by two X-ray crystallographic structures of the IL1β-S1 and IL1β-L3 constructs and for the remaining constructs by comparing the $^{1}H-^{15}N$ heteronuclear single-quantum coherence NMR spectra with that of the wild-type IL1β. Additionally, binding of LBT-loop IL1β proteins to their native binding partner in vitro remains unaltered. X-ray crystallographic phasing was successful using only the signal from the bound lanthanide. Large residual dipolar couplings (RDCs) could be determined by NMR spectroscopy for all LBT-loop constructs and revealed that the LBT-2 series were rigidly incorporated into the interleukin-1β structure. The paramagnetic NMR spectra of loop-LBT mutant IL1β-R2 were assigned and the $\Delta\chi$ tensor components were calculated on the basis of RDCs and pseudocontact shifts. A structural model of the IL1β-R2 construct was calculated using the paramagnetic restraints. The current data provide support that encodable LBTs serve as versatile biophysical tags when inserted into loop regions of proteins of known structure or predicted via homology modeling.

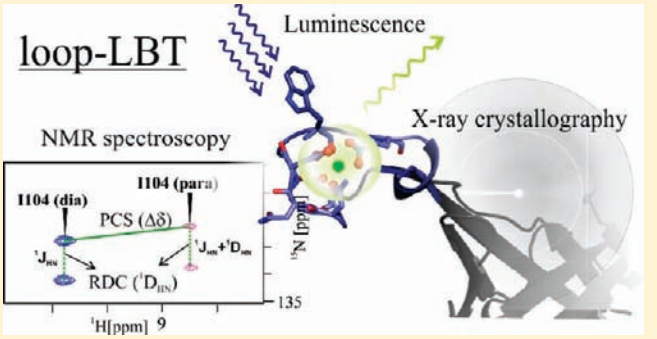

1. INTRODUCTION

Encoded peptide-based tags find widespread application in molecular, cellular, and structural biology.[1,2] The recently introduced lanthanide-binding tags (LBTs) represent a versatile class of such tags given their potential utility in luminescence-based measurements,[3] NMR spectroscopy,[4] and X-ray-crystallography.[5] The spectral characteristics of LBTs arise from the photophysical properties of the selected trivalent lanthanide (Ln) ions. In particular, Tb^{3+} and Eu^{3+} ions[6] are luminescent upon sensitization by organic fluorophores and exhibit distinct and long-lived[7] emission profiles, allowing cellular localization and binding interaction studies of LBT-tagged proteins.[8] The photophysical properties make lanthanide ions useful probes for imaging and resonance energy transfer experiments.[9,10] The indole side chain of tryptophan serves as a sensitizer to induce luminescence of the bound Tb^{3+} in LBTs.[11] In X-ray crystallography, lanthanides are used as heavy atoms and provide high phasing power due to their strong anomalous scattering that can be used for single- or multiple-wavelength anomalous phasing.[12−15] In NMR spectroscopy, the paramagnetic properties of lanthanide ions can be exploited to weakly align biomolecules along the magnetic field, leading to structural and dynamic restraints such as residual dipolar couplings (RDCs), pseudocontact shifts (PCSs), paramagnetic relaxation enhancement (PRE), or Curie cross-correlated relaxation (CCR).[16−24] These parameters have been shown to be sufficient to determine the overall fold of a protein even in the absence of nuclear overhauser effect (NOE) information. Compared to short-range distance restraints such as NOEs (<5 Å) and scalar couplings, RDCs provide long-range orientation information.[25] Additionally, PCSs can be used to determine structures of protein−protein and protein−ligand complexes.[26−29] Paramagnetic centers therefore augment the repertoire of methods which include liquid crystals,[30] polyacrylamide gels,[31] and phage[32] to induce partial alignment. The use of paramagnetic centers

Received: June 8, 2010
Published: December 23, 2010

overcomes the problem of external alignment interactions of the target protein with the media. In addition, the determination of relative domain motion in multidomain proteins or RNA strictly requires internal alignment to provide an independent frame of reference.[33,34]

The first biomolecular applications of paramagnetic alignment in NMR spectroscopy were introduced utilizing naturally occurring metal ion binding sites substituted with paramagnetic lanthanide ions[35] or a heme cofactor as the paramagnetic center bound to myoglobin.[36] In particular, similarities between the ionic radii of the divalent metal ions Ca^{2+}, Mg^{2+}, and Zn^{2+} and the trivalent lanthanide ions led to applications in which either one or two of these metal ions were replaced with paramagnetic lanthanide ions.[37,38] This approach was then extended to diamagnetic proteins lacking native metal-binding sites by fusion with entire paramagnetic protein domains such as zinc finger proteins,[39] EF hand motifs,[40] or calmodulin-binding peptides[16,41] loaded with paramagnetic lanthanide ions for alignment. However, use of such domains results in a considerable increase in molecular weight, which may cause a subsequent loss of signal intensity and also compromise the function of the protein. Furthermore, the high mobility of the tags relative to the protein scaffold reduces the extent of alignment and therefore may result in a low number of measurable structural restraints.[16]

Other strategies to introduce lanthanides exploited small organic metal-binding chelators based on diethylene triamine pentaacetic acid (DTPA),[42] ethylene diamine tetraacetic acid (EDTA),[43−45] or 1,4,7,10-tetraazacyclododecane-1,4,7,10-tetraacetic acid (DOTA)[46] attached to the protein via cysteine-modification chemistry. Although such chemical tags have been shown to induce alignment, they result in highly overlapping spectra due to peak doubling resulting from the diastereomeric nature of the tag.[19,47] Such chelators have also been stably attached at two points via cysteine disulfide bridges (CLaNP-5).[48,49] Additionally, the smallest known lanthanide-binding tag, diplicolinic acid (DPA) chelates the lanthanide ion using proximal carboxyl groups of the protein.[50] These tags need to be positioned carefully taking into account a suitable distance between the thiol group and nearest carboxyl group. Additionally, free cysteine thiols need to be available in the protein of interest or need to be engineered by site-directed mutagenesis.

Exploiting the strategy of paramagnetic protein fusion domains for alignment, a family of closely related single LBTs (sLBTs)[18] were designed by optimizing naturally occurring calcium-binding loops to avidly bind Ln ions.[51,52] These tags are short peptide sequences comprising up to 23 amino acids, which enable incorporation via standard molecular biology strategies. Design and engineering studies have resulted in tags that bind lanthanide ions tightly with low nanomolar K_D values and which are selective for lanthanides over other common metal ions.[53−56] Attached to either the N- or C-terminus, sLBTs were successfully introduced for NMR structure determination of proteins.[18,57] On the basis of previous investigations, the alignment induced by paramagnetic lanthanide ions was found to depend on the mobility of the tag relative to the protein frame.[25] Rigidification and site-specific tagging could also be achieved by linking an sLBT to a single cysteine within the protein via a disulfide bridge.[58,59] Two-point anchoring has been shown to further reduce the mobility of the tag compared to single-point anchoring.[60] However, this approach necessitates appropriate placement of a cysteine residue close to the N-terminus. The strategy using an encodable multifunctional peptide-based tag at the protein terminus was further improved by the design of a double LBT (dLBT) with two lanthanide binding motifs concatenated in a single 32-residue peptide.[5] The X-ray studies and NMR spectroscopic analysis of the subnanosecond dynamics of the tag[61] demonstrated that the increased tag size results in a less mobile tag that is sufficiently ordered with respect to the fusion protein ubiquitin. An increase in luminescence output was also shown for the dLBT-tagged ubiquitin fusion protein.[61]

In this study, we systematically investigate the possibility of further rigidifying LBTs with respect to the protein by incorporating an sLBT into defined loop regions. This design approach is based on our previous structure determination of Ln-bound LBTs. From these structural studies, we reasoned that integration of the LBT unit into proteins should be feasible with minimal disruption of the loop structures of the target protein. Therefore, the loop position and the length of the linker between the protein and the tag were systematically investigated using interleukin-1β (IL1β), a protein comprising three loops and a β-sheet core, as a model system. In the case of IL1β, the incorporation of the lanthanide-binding tag into any of three different protein loops did not impact the overall fold of the protein, the in vitro affinity for the native binding partner, or the binding affinity of Ln^{3+} to the LBT. In the present study we demonstrate a new and potentially general application of encoded lanthanide-binding tags.

2. RESULTS AND DISCUSSION

2.1. Design of IL1β−LBT. To utilize lanthanide-binding coexpression tags in NMR spectroscopy and in phasing for X-ray crystallography in macromolecular structure determination, the lanthanide tag must be well ordered with respect to the protein. A survey of structures deposited in the Protein Data Bank (PDB) reveals that, in over 50% of the structures submitted to the PDB, the N-terminal and/or C-terminal residues are disordered. These statistical studies suggest that, without significant interaction between the LBT and fusion protein or other means of decreasing domain−domain dynamics, the LBT might be ordered, but adopt several different orientations relative to the core of the protein of interest, therefore limiting its utility.

One method to reduce the conformational dynamics is to restrain both termini of the LBT to decrease interdomain motion, which could be achieved by making the LBT integral to the protein sequence. Although such placement requires some knowledge of either the secondary or tertiary structure of the protein, secondary structure prediction and homology modeling programs now allow for considerable accuracy in the prediction of β-turns from amino acid sequences. Therefore, it may be possible to predict appropriate placement of LBTs in structures on the basis of analyses of protein structures or directly from the protein sequence.[62,63] As a model system, the LBT was placed into three different loops (denoted L, R, and S) of IL1β differing in spacer length (denoted LBT-1−3) between the LBT and IL1β, resulting in nine different loop-LBT constructs (Table 1). The choice of the LBT sequence GYIDTNNDGWIEGDELY was based upon inspection of the crystal structure of ubiquitin with the dLBT tag.[5] Specifically, the termini of one terbium-binding loop were chosen so that they could insert into a pre-existing protein loop, allowing overlap of the two short β-strands of the dLBT with the native β-turn of the protein. It was envisioned that the metal-binding residues would remain appropriately positioned to

Table 1. Summary of IL1β−LBT Constructs, LBT Sequences, and K_D and q Values[a]

Construct	loop residue	IL1β -	LBT sequence	- IL1β	K_D (Tb^{3+}) [nM]	q
IL1β-S1	52-55	VQGEESN	GYIDTNNDGWIEGDELY	DKIPVAL	9.2 ± 0.8	0 ± 0.5
IL1β-S2	52-55	VQGEES-	GYIDTNNDGWIEGDELY	- KIPVAL	15.3 ± 1.3	0 ± 0.5
IL1β-S3	52-55	VQGEE-	GYIDTNNDGWIEGDELY	- - IPVAL	1.9 ± 0.1	0 ± 0.5
IL1β-L1	74-77	LSCVLKD	GYIDTNNDGWIEGDELY	DKPTLQL	3.8 ± 0.8	0 ± 0.5
IL1β-L2	74-77	LSCVLK-	GYIDTNNDGWIEGDELY	- KPTLQL	50.8 ± 2.3	0 ± 0.5
IL1β-L3	74-77	LSCVL- -	GYIDTNNDGWIEGDELY	- - PTLQL	1.31 ± 0.3	0 ± 0.5
IL1β-R1	138-141	FLGGTKG	GYIDTNNDGWIEGDELY	GQDITDF	13.2 ± 3.8	-
IL1β-R2	138-141	FLGGTK-	GYIDTNNDGWIEGDELY	- QDITDF	6.9 ± 1.4	-
IL1β-R3	138-141	FLGGT- -	GYIDTNNDGWIEGDELY	- - DITDF	17.2 ± 0.1	-

[a] Three constructs of each S-, L- and R-series were generated such that, in the LBT-1 series (IL1β-S1/L1/R1), the LBT was inserted between the middle loop residues. In the LBT-2 series (IL1β-S2/L2/R2), the flanking residues were removed and the LBT was inserted in their place. In the LBT-3 series (IL1β-S3/L3/R3), all four protein loop residues were removed and replaced by LBT. Dissociation constants (K_D) were determined by luminescence titration of LBTs by Tb^{3+} in 100 mM NaCl and 10 mM HEPES buffer at pH 7.0. All values are the average of at least three titrations. The number of bound water molecules, q, was determined by luminescence decay experiments (see the Materials and Methods).

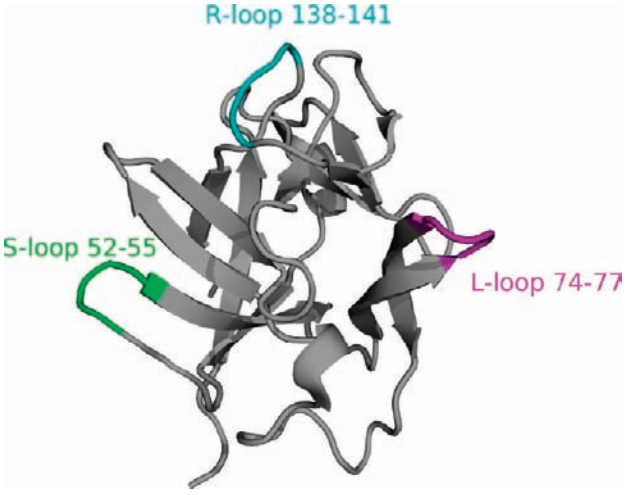

Figure 1. NMR structure of IL1β. sLBTs have been incorporated into three different loops shown here in purple for the L-loop (residues 74−77), in green for the S-loop (residues 52−55), and in cyan for the R-loop (residues 138−141).

bind the lanthanide without disrupting the protein fold. On the basis of published crystal and NMR structures of IL1β, three loops were identified as well suited for LBT insertion (Figure 1).[64,65] Previously, the S-loop was replaced in a similar, but not identical, position (residues 50−53 versus those replaced herein, 52−55) with the result that the protein was well folded, as assessed by NMR structure determination and the fact that the loop insertion (α-1-antitrypsin inhibitor) retained biological activity.[66] In this case, the construct did not have the same number of residues removed on either side of the loop and yet still folded robustly. This provides evidence that precise preknowledge of the loop structure is not an absolute requirement for the success of insert design.

An additional goal for incorporation of the tag was to retain binding affinity for the native IL1β receptor, IL-$1R_1$. For the S-series proteins, it is known from the literature that modification of this loop does not impair receptor binding, and binding is not related to the size of the inserted loop.[67] The second loop (L-series) targeted for LBT insertion is a β-turn. A previous cocrystal structure of IL1β with the IL1 receptor showed that this second loop is not involved in receptor recognition, and from computational studies it was predicted that it is also not involved in binding of an accessory protein.[64,68] Since residues 138−141 were also shown not to be involved in binding to the receptor, this loop was chosen for the third (R) series.[64,68,69] It is also known that derivatization of an IL1β-K138C mutant with iodoactamidofluorescein does not alter receptor recognition and that fusion with a large (275 kDa) protein did not significantly affect receptor binding.[69] Thus, inserting the relatively small LBT at this position may result in a construct retaining its ability to bind the receptor.

2.2. Preparation of IL1β-LBT. For luminescence measurements, NMR spectroscopy, and receptor-binding assays, full-length IL1β-S1−S3, IL1β-R1−R3, and IL1β-L1−L3 (the PDB entry for IL1β-S1 is 3LTQ, and that for IL1β-L3 is 3POK) were obtained via heterologous expression in *Escherichia coli* using a glutathione S-transferase (GST) fusion strategy for purification. For luminescence measurements and NMR spectroscopy, the expressed GST−IL1β−LBT proteins were cleaved with tobacco etch virus (TEV) protease at the inserted TEV site between the GST and IL1β and purified by size-exclusion chromatography to yield the desired LBT-tagged IL1β products.

For all NMR spectroscopic applications, ^{15}N-labeled proteins were expressed in P-5052 minimal-autoinduction media.[70] Expression of the R- and S-series resulted in very good yields of the soluble fusion protein (40−100 mg/L). In contrast, under the same conditions, proteins of the L-series were expressed as inclusion bodies in ^{15}N-minimal media. Therefore, the temperature was lowered to 16 °C, and proteins of the L-series were expressed in acceptable yields (ca. 20 mg/L; see the Supporting Information, Figure S1). Constructs of the S-series to be used for crystallization were expressed without a GST tag and refolded from inclusion bodies (see the Materials and Methods).

2.3. Receptor-Binding Assays. The IL1 proteins including IL1α and IL1β are proinflammatory cytokines, which participate in the regulation of numerous immunological and inflammatory processes.[71] To control biological activity of IL-1, initiation of signal transduction occurs upon binding of agonist ligands (IL1α or IL1β) to a specific membrane receptor, the transmembrane glycoprotein of the immunoglobulin superfamily IL-$1R_1$.[72]

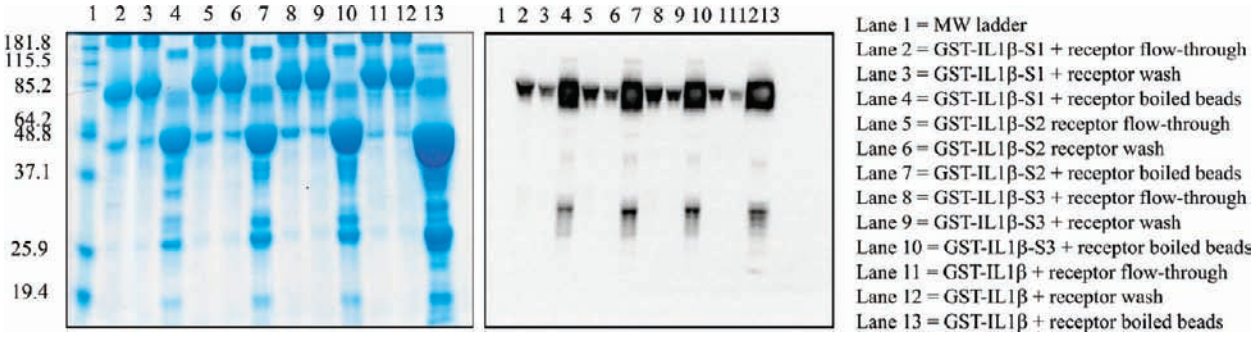

Figure 2. Receptor-binding assay results, with representative 12% SDS−PAGE gel (left) and anti-sIL-1R$_1$ Western blot (right) shown for GST−IL1β-S1, -S2, and -S3. All experiments were performed in 10 mM HEPES, 100 mM NaCl, pH 7.0, with 0.1% BSA. A 1 mg portion of each protein was preloaded with 1 equiv of Tb^{3+}.

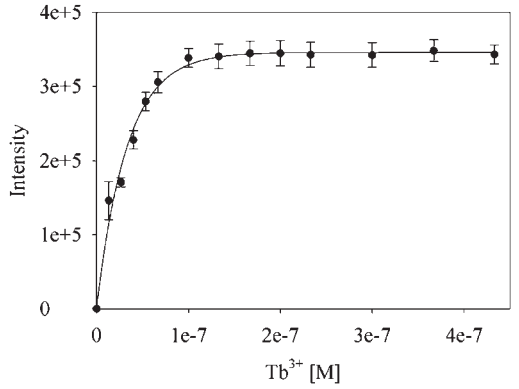

Figure 3. Tb^{3+} titration data and fit, shown for IL1β-R1. The data points represent the average of three independent measurements.

Receptor-binding studies were performed using a pull-down assay, in which GST IL1β−LBT bound to glutathione Sepharose beads served as bait for the soluble receptor s-IL-1R$_1$. As confirmed by sodium dodecyl sulfate-polyacrylamide gel electrophoresis (SDS−PAGE) and Western blot analysis (see the Supporting Information, Figures S2 and S3), the incorporation of the LBT does not impair the receptor-binding capability of the engineered loop-LBT IL1β mutants. Representative data for the IL1β-S-series are shown in Figure 2 (lanes 4, 7, and 10).

2.4. Photophysical Characterization. We determined the luminescence properties and the number of Tb^{3+}-bound water molecules of the LBT-tagged constructs. Luminescence titration studies revealed that the LBTs in all three insert sites bind Tb^{3+} tightly, with binding constants in the low nanomolar range (Figure 3 and Table 1). The binding affinity of Tb^{3+} to the loop-LBTs is similar to those found for the first binding event of Tb^{3+} binding to the dLBT.[18,61] While IL1β-L2 shows a slightly higher dissociation constant, we note that two positively charged lysine residues flank the LBT incorporation site in this construct. It is possible that the positively charged side chains surrounding the LBT slightly impede binding of Tb^{3+}. From these results, it can be concluded that covalently linking the LBT into protein loops does not compromise the binding affinity for Tb^{3+}.

LBTs were originally developed to exclude water from the lanthanide coordination sphere, since coordinated water molecules cause excited Tb^{3+} to undergo rapid, nonradiative energy transfer to the vibrational states of the water O−H bonds, leading to a decrease in the luminescence intensity and lifetime.[73] The number of bound water molecules was thus evaluated for six of the nine IL1β−LBT proteins (see Table 1 and the Supporting Information, Figure S4) using standard methods.[74] It was confirmed that there are no water molecules bound to the metal center in any of the loop-LBT proteins as shown by near-zero q values (Table 1). These findings are consistent with data reported previously for sLBTs and dLBTs.[61]

2.5. Characterization of Loop-LBT by NMR Spectroscopy. In solution, dipolar couplings are averaged to zero due to molecular tumbling. Lanthanides with an anisotropic magnetic susceptibility tensor $\Delta\chi$ induce partial alignment within the magnetic field, leading to RDCs.[25] The RDC between two heteronuclear nuclei A and B, D_{AB}, is described by

$$D_{AB}(\theta,\phi) = -\frac{\gamma_A\gamma_B\mu_0 S\hbar}{8\pi^2 r_{AB}{}^3}\left[A_a(3\cos^2\theta-1)+\frac{3}{2}A_r\sin^2\theta\cos 2\phi\right] \quad (1)$$

where θ and φ describe the orientation of the internuclear vector in the principal axis system of the alignment tensor, A_a and A_r are the axial and rhombic components of the alignment tensor, r_{AB} is the internuclear distance, S is the generalized order parameter, γ_A and γ_B are the gyromagnetic ratios of nuclei A and B, $\hbar$ is Planck's constant divided by 2π, and μ_0 is the magnetic permeability of a vacuum.[25,59]

Furthermore, PCSs $(\delta\Delta)$[75] induced by the anisotropic magnetic susceptibility of paramagnetic centers correspond to a change in the observed chemical shifts between paramagnetic and diamagnetic samples that depend on the distance and position relative to the paramagnetic center and are described by

$$\delta\Delta = \frac{1}{12\pi r^3}\left[\Delta\chi_a(3\cos^2\theta-1)+\frac{3}{2}\Delta\chi_r\sin^2\theta\cos 2\varphi\right] \quad (2)$$

where $\Delta\chi_a$ and $\Delta\chi_r$ are the axial and rhombic components of the anisotropic magnetic susceptibility tensor describing the magnetic moment of the paramagnetic center and r, θ, and φ are the spherical coordinates of the nucleus in the frame of the $\Delta\chi$ tensor.[76]

The alignment tensor is proportional to the $\Delta\chi$ tensor:

$$A_{a,r} = \frac{\mathbf{B}_0{}^2}{15\mu_0 k_B T}\Delta\chi_{a,r} \quad (3)$$

where $\mathbf{B}_0$ is the external magnetic field, k_B is the Boltzmann constant, T is the temperature (K), and $\Delta\chi_{a,r}$ are the axial and rhombic components of the anisotropic magnetic susceptibility

dx.doi.org/10.1021/ja104983t | J. Am. Chem. Soc. 2011, 133, 808–819

tensor. The observed RDCs depend on the magnetic field strength $\mathbf{B}_0^2$ and the $\Delta\chi_a$ and $\Delta\chi_r$ for the different lanthanides.[59,77]

Paramagnetic properties differ between lanthanides.[75] Therefore, the extent of alignment and observed RDC and PCS can be fine-tuned by the choice of paramagnetic ion. The peptide-based LBTs bind Tb^{3+}, Tm^{3+}, Er^{3+}, Lu^{3+}, La^{3+},Dy^{3+}, Yb^{3+}, and Ho^{3+}, and NMR studies were performed for the described lanthanide ions.[18,57−61] The possibility of measuring RDCs for LBTs as fusion tags was first shown for sLBTs and dLBTs attached to the N-terminus of ubiquitin using Tm^{3+} as the paramagnetic ion. Compared to the sLBT, an additional β-sheet was formed in the structure of the dLBT peptide chain, which resulted in decreased tag flexibility and improved alignment. For the sLBT, RDC values between −2 and +6 Hz could be measured on a spectrometer with a ^{1}H frequency of 800 MHz. The size of the RDC was increased for the dLBT by a factor of 3 with RDCs in the range of −18 to +12 Hz due to the decreased mobility of the tag relative to the protein as inferred from analysis of order parameters from ^{15}N relaxation data. For the sLBT complexed with Tb^{3+}, RDCs were observed between −7.6 and +5.5 Hz.

Previous studies have shown that fusion to the highly flexible N- and C-termini limits the possible attachment sites and does not confer maximum rigidity of the tag. Attaching the sLBT sequence via a disulfide linkage to a cysteine residue yielded RDC values from −12 to +21 Hz for Tm^{3+} at 800 MHz. Recently, increased rigidification could also be achieved by linking the sLBT via two anchoring points, providing RDC values in the range of −12 to +11 Hz for Tb^{3+} at 600 MHz.[60] The present study was conducted to improve the rigid attachment of the sLBT. NMR analyses were performed for all nine IL1β−LBT constructs in the IL1β-R, -S, and -L series. We titrated ^{15}N-labeled protein with a 1.1-fold excess of paramagnetic Tb^{3+} and Tm^{3+} ions or Lu^{3+} ions as a diamagnetic reference. Paramagnetic shifts and signal broadening could be observed in the ^{1}H−^{15}N heteronuclear single-quantum coherence (HSQC) spectra of the paramagnetic protein complexes, demonstrating the utility of loop-LBTs for the measurement of paramagnetic effects.

2.5.1. Magnitude of Observed RDCs. RDC values for the amide ^{1}H−^{15}N backbone amide spin pairs ($^1D_{HN}$) were obtained by subtracting the scalar coupling ($^1J_{HN}$) in the presence of diamagnetic Lu^{3+} from the sum of scalar and dipolar coupling in the presence of paramagnetic Tb^{3+}, both measured in ^{1}H−^{15}N IPAP-HSQCs. Large RDC values could be observed for the IL1β-S-series in the range of −14 to +18 Hz for Tb^{3+}, for the IL1β-R-series in the range of about −12 to +12 Hz, and for the IL1β-L-series in the range of −16 to +18 Hz at 600 MHz. Additionally, RDCs were measured for the loop mutant IL1β-R2 using Tm^{3+} as a second paramagnetic lanthanide ion. RDCs with values from −12 to +10 Hz were observed (see the Supporting Information, Figure S6). Compared to RDC values of sLBT, the loop-LBTs provide a more than 3-fold improvement, demonstrating that the LBT is rigidly attached within the protein frame. Furthermore, the RDC values depend on the linker length, where the LBT-2 series was found to be optimal (Figure 4).

To make use of RDCs for structure refinement, the magnitude of the axial component of the molecular alignment tensor and the rhombicity must be known. A generalized expression for the RDC can be described by

$$D_{AB}(\theta,\phi) = D_a^{AB}\left[(3\cos^2\theta - 1) + \frac{3}{2}R\sin^2\theta\cos 2\phi\right] \quad (4)$$

where D_a is the magnitude of the residual dipolar coupling tensor with $D_a^{AB} = -(B_0^2h/60kT\pi^2)S\gamma_A\gamma_B\langle r_{AB}^{-3}\rangle\chi_a$ and R the rhombicity.[78,80] The histogram of the ensemble of RDCs approximates a powder pattern from which D_a^{NH} and R are readily extracted in the absence of any prior structural information for all IL1β−LBT loop constructs.[78,80,81] The histograms for the IL1β-S, -R, and -L series suggest asymmetric shapes of the molecules with calculated values for the rhombicity greater than zero ($R > 0$) (Figure 4).

2.5.2. Diamagnetic Assignment of the Loop-LBT Construct IL1β-R2. To assign the ^{1}H−^{15}N HSQC cross-peaks of the diamagnetic spectra of IL1β-R2, a 3D ^{1}H−^{15}N NOESY-HSQC was recorded and assigned utilizing the known assignments of wt-IL1β.[82] The similarity of the ^{1}H−^{15}N HSQC spectra of wt-IL1β and the LBT insertion mutants shows the minimal structural perturbation induced by the LBTs onto the protein structure (see the Supporting Information, Figure S5). Additional peaks for the LBT sequence could be detected by comparing the diamagnetic spectra with a reference sample missing the lanthanide ion. In this sample, 89% of the backbone amide signals of diamagnetic spectra could be assigned. Figure 5 shows the paramagnetic and diamagnetic ^{1}H−^{15}N HSQC spectra of IL1β-R2. The effects of the paramagnetic lanthanide ion are shown in representative one-dimensional traces for residues N119, I104, and M44 because residues in close proximity to the lanthanide ion experience larger paramagnetic effects than those more distant from the paramagnetic center.

2.5.3. Paramagnetic Assignment of the Loop-LBT Construct IL1β-R2. The ^{1}H−^{15}N HSQC cross-peaks of the paramagnetic spectra were assigned using the diamagnetic assignment. The resonances in the ^{1}H−^{15}N HSQC spectra for Tb^{3+}, Tm^{3+}, and the diamagnetic sample with Lu^{3+} are displaced on diagonal lines due to the similarity of the PCS values of the bonded ^{1}H and ^{15}N spins by which most of the paramagnetic shifts could be assigned (Figure 5).[83] Signals that initially remained unassigned were assigned using a bootstrapping procedure. The initial experimental PCS values were used to predict a first position of the lanthanide ion on the basis of the wild-type crystal structure (PDB entry 9ILB) using the program Numbat.[84] Prediction of the unassigned PCSs onto the wild-type crystal structure was achieved using the program Echidna,[83] where the initial lanthanide position, the diamagnetic assignment, and the peak table of the paramagnetic ^{1}H−^{15}N HSQC including some of the reliable and unambiguously assigned paramagnetic peaks were used as input data.[84] The iterative procedure resulted in the assignment of 102 out of 140 of the backbone amide cross-peaks peaks for the spectrum with Tb^{3+} and 99 cross-peaks for Tm^{3+}. PCS values of up to 1 and 0.6 ppm could be detected for Tb^{3+} and Tm^{3+}, respectively (see the Supporting Information, Table S2).

A cross-validation of the experimental RDCs showed a correlation of 0.93 with the three-dimensional crystal structure of native IL1β (PDB entry 9ILB) using the program PALES.[79] A structure minimization was performed using the crystal structure of native IL1β and the previously optimized alignment tensor parameters for Tb^{3+} showing only small changes (see Supporting Information, Figure S6). Cross-validation of the final experimental RDCs and PCS values showed an excellent fit with the refined crystal structure of wt-IL1β (Figure 6a). The $\Delta\chi$ tensor values were then calculated on the basis of the PCS values and the refined wild-type crystal structure. These values are, however, smaller than those reported in the literature, the reason for which remains unclear.[85] The data were proven to be robust by

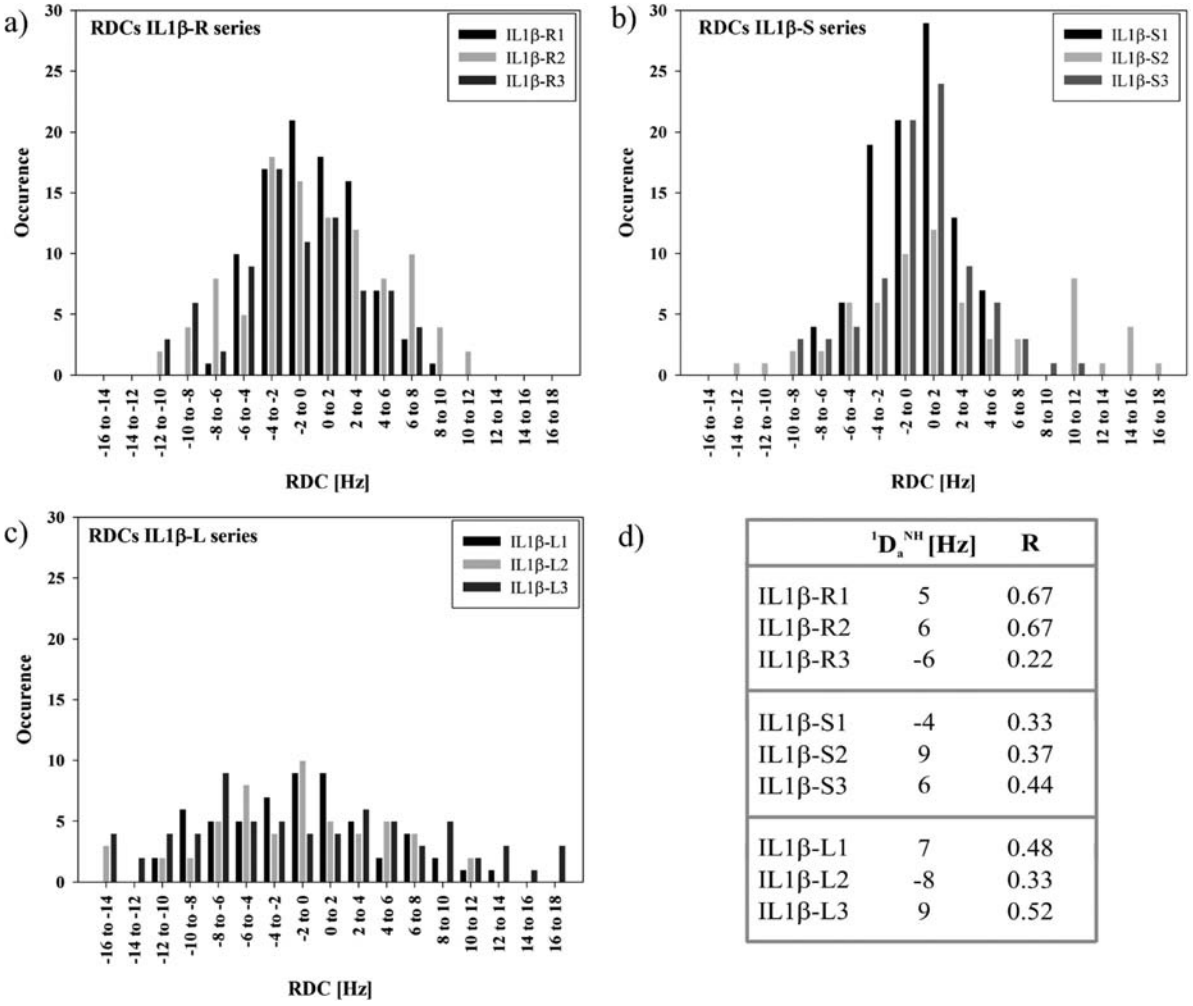

d)

	$^1D_a^{NH}$ [Hz]	R
IL1β-R1	5	0.67
IL1β-R2	6	0.67
IL1β-R3	-6	0.22
IL1β-S1	-4	0.33
IL1β-S2	9	0.37
IL1β-S3	6	0.44
IL1β-L1	7	0.48
IL1β-L2	-8	0.33
IL1β-L3	9	0.52

Figure 4. (a) RDC histogram for IL1β-S1, -S2, and -S3. (b) RDC histogram for IL1β-R1, -R2, and -R3. (c) RDC histogram for IL1β-L1, -L2, and -L3. (d) . Estimated values of D_a^{NH} and R are obtained by nonlinear least-squares optimization of the equations $D_{zz}^{NH} = 2D_a^{NH}$, $D_{yy}^{NH} = -D_a^{NH}(1 + 1.5R)$, $D_{xx}^{NH} = -D_a^{NH}(1 - 1.5R)$, and $R = D_r^{NH}/D_a^{NH}$. The values of D_{zz}, D_{yy}, and D_{xx} were measured from the histograms of the RDCs for IL1β−LBT by taking the extreme high and low values such that $|D_{zz}^{NH}| > |D_{yy}^{NH}| \geq |D_{xx}^{NH}|$. D_{xx} corresponds to the most populated value in the histogram of the RDCs.[78,79]

performing a Monte Carlo error analysis where 30% of the experimental PCSs were randomly deleted. The Monte Carlo error analysis and the principal tensor axis orientations are shown in Sanson−Flamsteed projections. Additionally, using the assigned PCS values, perfect metal ion positions located adjacent to the R-loop were calculated with an optimal distance of 10 Å with respect to the loop residues. Alignment tensors for IL1β-R2 with Tb^{3+} were calculated on the basis of the RDC values and the refined crystal structure of wt-IL1β using the program PALES.[79] To compare the RDC and PCS data sets, the alignment tensor was converted to the $\Delta\chi$ tensor using eq 2. The result shows a $\Delta\chi_a^{RDC}$ tensor scaled by 20−30% in comparison with $\Delta\chi_a^{PCS}$. The RDCs seem to be more sensitive to the mobility of the lanthanide ion than the PCS values (Figure 6); such observations have been previously discussed.[86]

2.5.4. Model of the Loop-LBT Construct IL1β-R2. In an effort to invert the iterative assignment procedure, we modeled the structure of the loop from experimental RDCs, diffusion anisotropy, and PCSs using the program CNS.[87] The X-ray crystal structure of IL1β (PDB entry 9ILB) was used as the starting structure. Distance information calculated for the lanthanide position from PCS values using Numbat[84] and the experimental RDCs were used as restraints. Calculation of the loop-LBT IL1β-R2 model structure was performed keeping the stable secondary structure core parts of the molecule by fixing the heavy atom coordinate positions and by the addition of hydrogen bond restraints. On the basis of the X-ray crystal structure of IL1β-S1 (vide infra), heavy atom distance restraints were added for the LBT and the lanthanide ion to keep the structure of the tag intact. The linker region of the tag was fully unrestrained. Figure 7 shows the final calculated model of the loop-LBT construct IL1β-R2. Following the calculation, a cross-validation of the model was performed using the paramagnetic restraints in Numbat.[84] The back-calculated PCS for the backbone amide protons are in excellent agreement with the model. In addition, the overlay of the lanthanide position resulting from the model and from the Numbat back-calculated position is in excellent agreement and gives further support for the calculated model of IL1β-R2 and to the applicability of loop-LBTs for protein structure determination.

Spin−lattice ^{15}N R_1 and spin−spin ^{15}N R_2 relaxation rates as well as the heteronuclear $\{^1H\}-^{15}N$ nuclear Overhauser effect were measured for most backbone amide groups of loop-LBT IL1β-R2 and used to calculate the general order parameter S^2, characterizing the amplitude of internal amide bond vector motion on time scales faster than the overall correlation time τ_c, by

dx.doi.org/10.1021/ja104983t |J. Am. Chem. Soc. 2011, 133, 808–819

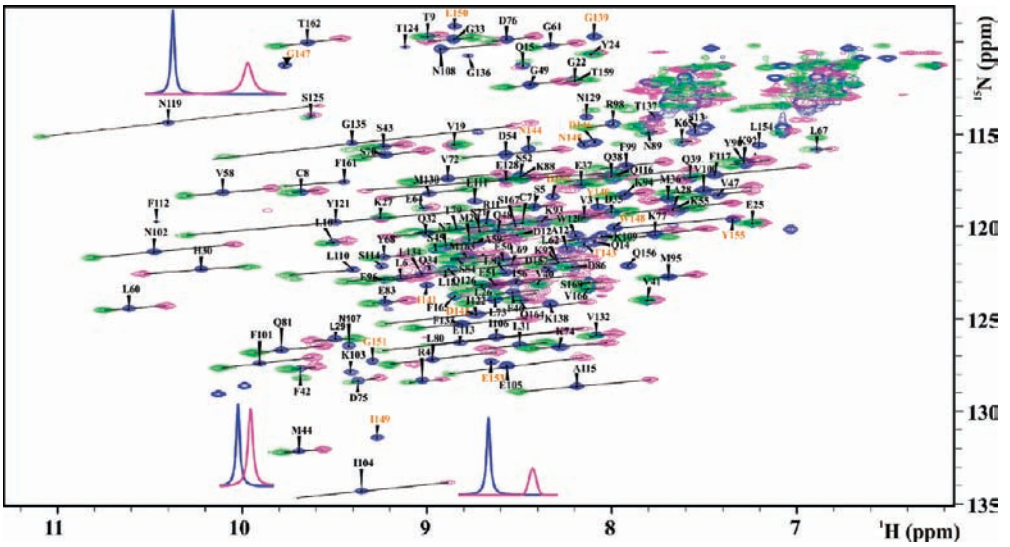

Figure 5. ^{1}H−^{15}N HSQC spectrum showing the assigned backbone amide resonances of the sLBT-tagged interleukin-1β-R2 in the presence of 1.1 equiv of diamagnetic Lu^{3+} (blue) and paramagnetic Tb^{3+} (pink) and Tm^{3+} (green). PCS vectors are indicated as black lines between corresponding diamagnetic and paramagnetic peaks. 1D spectra from the diamagnetic (blue) and paramagnetic (pink, Tb^{3+}) experiments are shown for representative resonances, indicating a paramagnetic shift and signal broadening. Additional peaks resulting from the LBT sequence are annotated in orange.

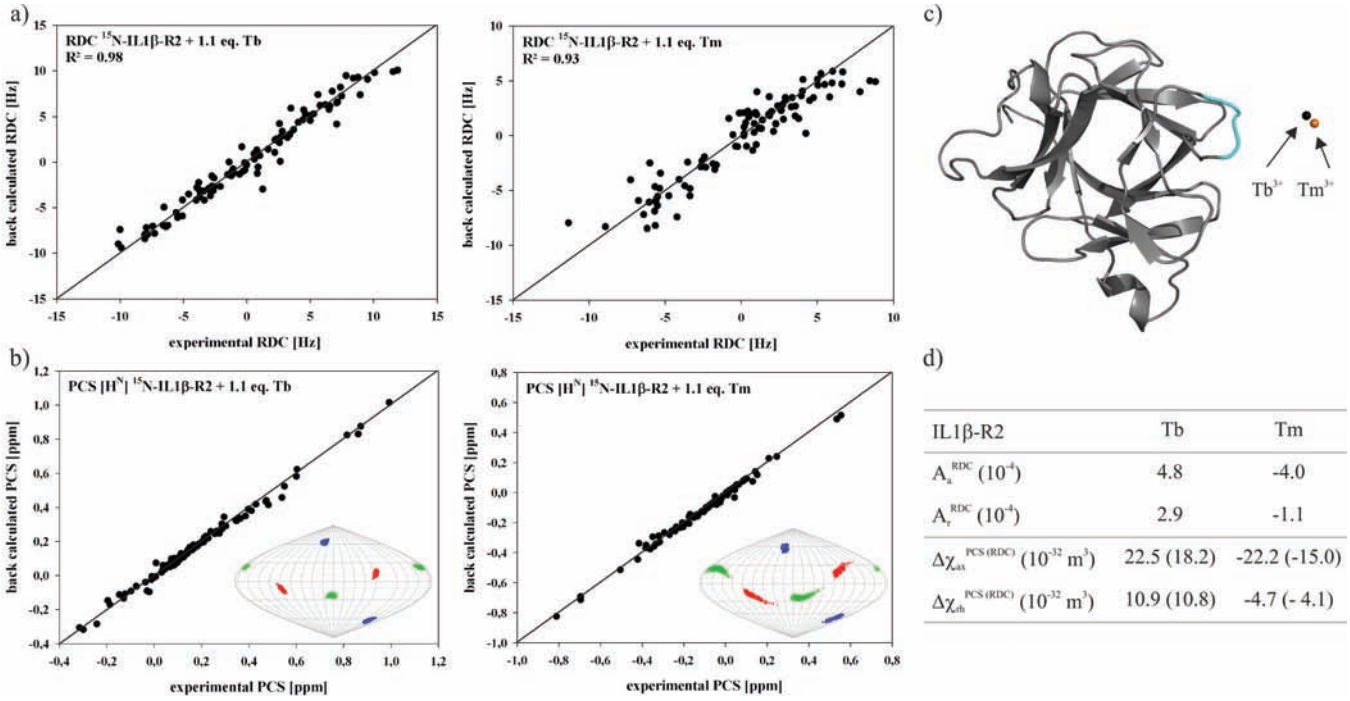

IL1β-R2	Tb	Tm
A_a^{RDC} (10^{-4})	4.8	-4.0
A_r^{RDC} (10^{-4})	2.9	-1.1
$\Delta\chi_{ax}^{PCS\ (RDC)}$ (10^{-32} m^3)	22.5 (18.2)	-22.2 (-15.0)
$\Delta\chi_{rh}^{PCS\ (RDC)}$ (10^{-32} m^3)	10.9 (10.8)	-4.7 (- 4.1)

Figure 6. (a) Scatter plot showing the correlation between observed $^{1}D_{HN}$ dipolar shifts (Hz) for loop-LBT mutant IL1β-R2 and those back-calculated using the program PALES[79] on the basis of the refined crystal structure of Il1β (PDB entry 9ILB). (b) Cross-validation of the final experimental PCSs using Numbat.[84] Orientations of the $\Delta\chi$ tensor axis components of Tb^{3+} in complex with IL1β-R2 are visualized in Sanson−Flamsteed projections with the *z*-, *y*-, and *x*-axes in blue, green, and red, respectively. A total of 500 sets of plots represent the result of the Monte Carlo error analysis in which 30% of the data were randomly deleted. (c) The position of the lanthanide ion with respect to the protein is indicated as a black sphere for Tb^{3+} and as an orange sphere for Tm^{3+}. (d) The calculated axial and rhombic components of the anisotropic magnetic susceptibility ($\Delta\chi$) tensor and the alignment tensor based on the refined crystal structure of IL1β (PDB entry 9ILB).

a Lipari−Szabo analysis[88,89] with the program TENSOR2[90] using an anisotropic diffusion tensor (Figure 8).

Mean order parameters for loop-LBT IL1β-R2 show lower values for the loop-LBT residues than those of the remaining protein, indicating some mobility of the loop residues (G139−Y155) compared to the β-sheet core structure of IL1β. However, these values are on the same order as those for the dLBT sequence.[61] The increased dynamics in the loop-LBT residues might account for the measured $\Delta\chi$ tensor values resulting in averaged tensor values.

dx.doi.org/10.1021/ja104983t |*J. Am. Chem. Soc.* 2011, 133, 808–819

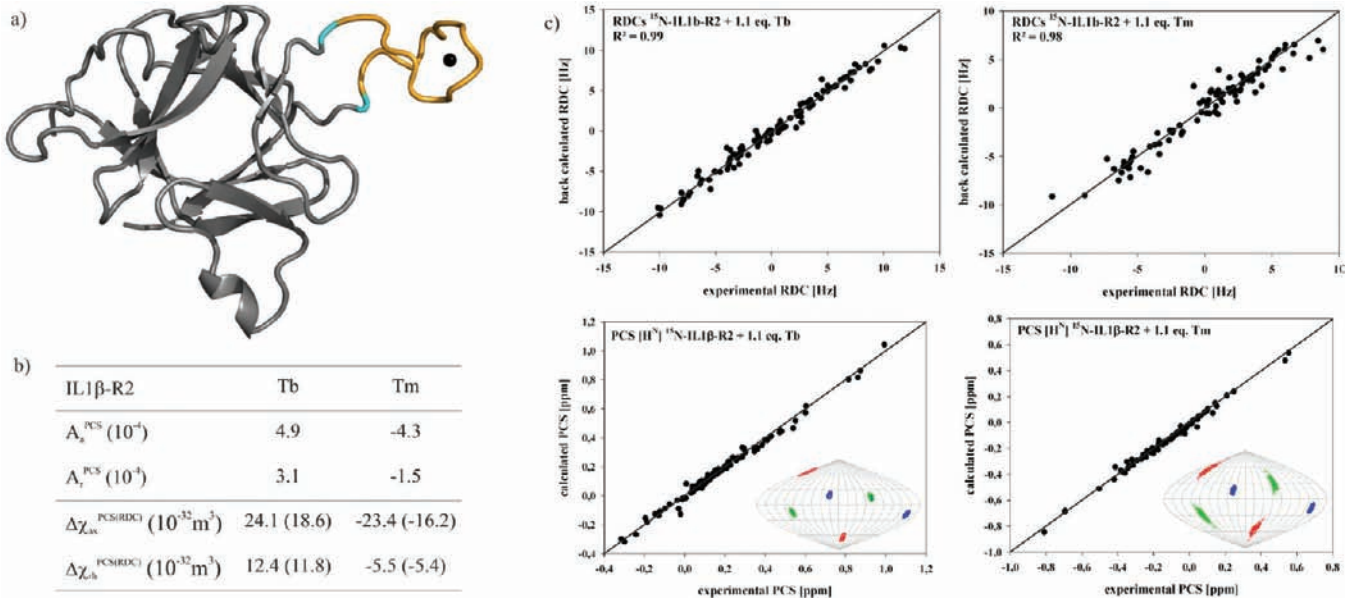

Figure 7. (a) Model of the loop-LBT IL1β-R2 with the metal position indicated as a black sphere. (b) From PALES[79] and Numbat[84] estimated alignment tensor and $\Delta\chi$ tensor values. (c) Scatter plot showing the correlation between observed $^1D_{HN}$ dipolar shifts (Hz) and those back-calculated using the program PALES[79] on the basis of the model of IL1β-R2. (d) Cross-validation of the final experimental PCS values using Numbat.[84] Orientations of the $\Delta\chi$ tensor axis components of Tb^{3+} in complex with IL1β-R2 are visualized in Sanson−Flamsteed projections with the *z*-, *y*-, and *x*-axes in blue, green, and red, respectively. A total of 500 sets of plots represent the result of the Monte Carlo error analysis in which 30% of the data were randomly deleted.

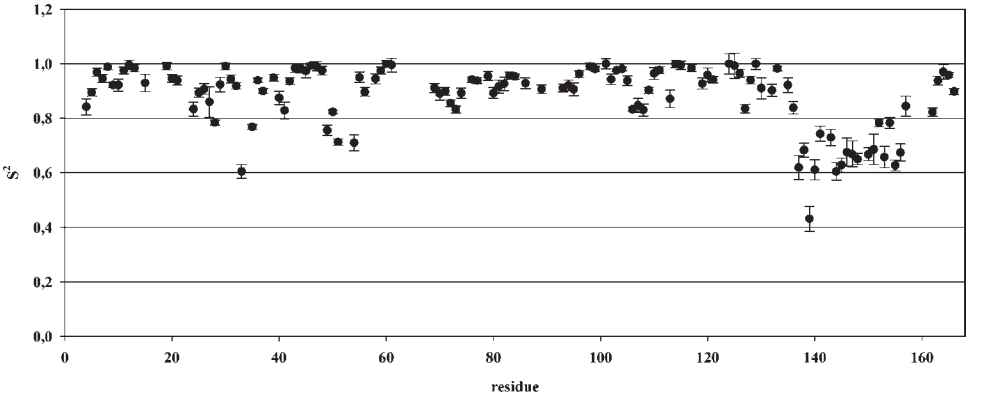

Figure 8. Generalized order parameters S^2 for the $^1H-^{15}N$ amide bond vector shown for loop-LBT IL1β-R2. Analysis was performed using the program TENSOR2. An overall τ_c of 11.49 ns and an axially symmetric diffusion tensor were determined with an asymmetry of 1.37.

2.6. Characterization of IL1β-S1 by X-ray Crystallography. *2.6.1. Comparison to Native IL1β and Known LBT Structures.* The structure of IL1β-S1 complexed with Tb^{3+} (Figure 9) determined by X-ray crystallography comprises an IL1β with the LBT domain inserted at the end of a pair of antiparallel β-sheets. The structure of IL1β is essentially unchanged. Notably, initial phasing was accomplished utilizing only the anomalous scattering from the bound Tb^{3+}. Comparison of the structure of IL1β-S1 to that of the known 1.5 Å IL1β structure (PDB accession code 2NVH) shows an rmsd of 0.918 Å for 152 of 153 residues. The largest deviations are found in residues 32−34, 105−109 (both surface turns), and 49−53. The 49−53 stretch leads up to the insertion with a C_α displacement of 1.6−3.3 Å. Notably, after the insertion point and the first atom of residue 54, the displacement is only 0.2−0.6 Å. Thus, no significant change in the fusion protein occurs from insertion of the LBT, as shown by the X-ray crystallographic structure. Only some minor, local deviations are apparent at the insertion site itself. The generality of the finding that the LBT does not affect the scaffold protein structure is also supported by the X-ray crystallographic structure determination of IL1β-L3 to 1.7 Å resolution (Supporting Information, Table S4). The LBT loop in this structure showed disorder (7 of the 17 LBT residues could not be modeled, and the lanthanide could not be built into the electron density). However, the overall protein fold does not differ from that of wild-type IL1β with rmsd = 0.87 Å. The observed disorder in the LBT electron density in IL1β-L3 is also consistent with the conclusion from NMR that the mobility of the LBT is dependent on the insertion topology.

The LBT inserted into the IL1β-S1 construct was designed on the basis of the structure of the double LBT domain from the dLBT−ubiquitin structure. The rmsd of the 20 matching atoms

dx.doi.org/10.1021/ja104983t |*J. Am. Chem. Soc.* 2011, 133, 808–819

Figure 9. (a) Crystal structure of IL1β-S1 colored from the N-terminus (red) to the C-terminus (blue). (b) Overlay of the IL1β-S1 model (green) on the reference 2NVH (red). (c) IL1β-S1 structure colored by temperature factor (blue, low, to red, high). The LBT (inserted into the S-loop) is marked by the Tb^{3+} depicted as a sphere.

Figure 10. Overlay of the LBT portion of IL1β-S1 (red) with the dLBT portion of the ubiquitin structure (green) showing how the dLBT forms a pair of antiparallel β-strands which fit into the β-sheet of IL1β.

of the IL1β-S1−LBT and the dLBT is 0.682 Å. Therefore, the structure of the LBT is essentially unchanged in the environment of the insertion site in the protein (Figure 10).

2.6.2. B-Factor Analysis. In a typical globular protein, the temperature factors of atoms in the model are lower in the core of the protein and increase radially from the center, reflecting the mobility inherent in the protein. Such is the case with the reference IL1β (PDB entry 2NVH). However, in the IL1β-S1 model, the relatively low *B*-factors in the core are shared by those residues in the LBT. The atoms of the LBT domain have temperature factors of 11−17 $Å^2$ compared to the overall average *B*-factor of 31 $Å^2$ for the entire structure. The lower values are for atoms chelating the Tb^{3+} and the tryptophan which makes a crystal contact. This is consistent with the LBT domain acting like a "core". The stability of the LBT domain allows for the scattering from Tb^{3+} to be used for phasing. Additional stability is afforded by crystal packing interactions between IL1β molecules.

2.6.3. Crystal Packing. With any X-ray crystal structure, one must be cognizant of the role that crystal packing may have on the target molecule. In this structure, as in the dLBT−ubiquitin model, the tryptophan of the LBT fits into a groove of a hydrophobic pocket created by the symmetry-related molecule, thereby stabilizing and immobilizing the LBT. The pocket is formed on the face of the symmetry-related 105−109 region, which also showed a 1.0−3.9 Å displacement relative to the reference model 2NVH. Although the relative mobility of the LBT is restricted in this design by the insertion into a β-turn, a potential additional source of stability is the formation of this crystal contact. However, the results from NMR presented herein reflect the low mobility in solution of the LBT domain in these fusion proteins and rule out crystal contacts as the primary source of interdomain stability.

3. CONCLUSIONS

Overall, this study provides a comprehensive analysis of the effect of inserting LBTs into protein loops, using the model protein IL1β. Analysis of the loop position shows that a canonical β-turn or loop motif provides a suitable insertion site. Luminescence studies demonstrate that the binding affinity is not correlated to loop mobility (determined by NMR) and is fairly insensitive to the flanking sequence or to the length of the spacer between LBT and protein. However, effects correlated with motion as assessed by NMR show that the LBT-2 series (IL1β-S2, -R2, and -L2) is superior in terms of conferring a low relative mobility of the LBT with respect to the fusion partner.

Through a systematic analysis, we show that LBTs are versatile tools for the exploitation of the photophysical, paramagnetic, and diffraction properties of lanthanides in NMR and crystallographic structure determination and luminescence applications. LBTs can be attached to proteins via the N-terminus and/or C-terminus, attached to one or two cysteine side chains, or, as shown here, incorporated into loop regions of proteins, relying on well-established molecular biology protocols. For IL1β, incorporation of the LBT impairs neither the overall fold of the protein nor the binding affinity of Ln^{3+} to the LBT. As such, the insertion of an LBT can be used for phasing via X-ray crystallography. Furthermore, the loop insertion does not impair binding of IL1β to the soluble domain of the cognate receptor. Incorporation of LBTs into loop regions of proteins provides a broadly applicable strategy for protein research. Such an improved toolkit is of importance to future applications in phase determination in X-ray crystallography and for the structure determination of large protein complexes by NMR where the LBT can be fused into one NMR-silent binding partner without increased mobility in a similar manner.

4. MATERIALS AND METHODS

4.1. Preparation of IL1β−LBT. Starting from a plasmid encoding human IL1β obtained from ATCC (S595), the cloning of IL1β-S2, -L2, and -R2 was accomplished via a two-step polymerase chain reaction (PCR) procedure. First, the two halves of IL1β were separately amplified by PCR, with primers that included overhangs encoding the desired LBT (GYIDTNNDGWIEGDELY). The two PCR fragments

contained complementary sequences at their termini that could be annealed to each other. Extension via PCR then yielded a product encoding full-length IL1β-S2, -L2, or -R2 with the LBT at the desired position. This insert was then inserted into the vector pGEX-4T-2. A TEV protease cleavage site (ENLYFQM) was included to facilitate removal of the N-terminal GST fusion protein. The final construct expresses GST−ENLYFQM−IL1β(LBT). To generate IL1β-S1 and IL1β-S3, site-directed mutagenesis was used to insert or remove codons corresponding to the appropriate amino acids (see Table 1). IL1β-R1 and -R3 were similarly generated from IL1β-R2, and IL1β-L1 and -L3 were similarly generated from IL1β-L2.

Initially, proteins were expressed using isopropyl β-D-1-thiogalactopyranoside (IPTG) induction with excellent protein yields of ~25−50 mg/L, identified by SDS−PAGE, and purified using glutathione Sepharose. The temperature for ITPG-induced protein expression was lowered to 16 °C since expression at higher temperatures led to truncation products. Improved yields could be obtained using the Studier auto-induction method for protein expression.[70] The proteins were expressed in BL21-CodonPlus(DE3)-RIL using ZYM-5052 complex autoinducing media with excellent yields of about 40−200 mg/L. Protein expression was conducted overnight at 37 °C, resulting in no significant truncation products. Following purification on glutathione Sepharose, the GST−IL1β−LBT proteins were cleaved with TEV protease and purified by size-exclusion chromatography to yield the desired LBT-tagged IL1β products. For protein expression of the L-series the temperature was lowered to 16 °C to avoid expression in inclusion bodies.

For crystallization experiments, constructs of the S-series were cloned starting from IL1-AT(4), which was kindly provided by Prof. T. Pochapsky, Brandeis University, Waltham, MA. The gene encoding IL1β was modified to remove the chymotrypsin recognition site, insert the LBT domain, and transfer the gene to a pET3a vector with a T7 promoter for IPTG-inducible expression. Standard molecular biology tools were used via a QuickChange protocol to insert the LBT using an "inchworm technique", adding approximately one-third of the LBT with each round of modification. Plasmids were sequenced at the Tufts University Core Facility, Medford, MA.

4.2. Luminescence Titrations. Titrations were recorded on a Fluoromax-3 spectrometer (Jobin Yvon Horiba) in a 1 cm path length quartz cuvette. Tryptophan-sensitized Tb^{3+} emission spectra were collected by exciting the sample at 280 nm and recording the emission at 544 nm. A 315 nm long-pass filter was used to avoid interference from harmonic doubling. Slit widths of 5 nm were used with 1 s integration times. Luminescence spectra were recorded at room temperature and were corrected for intensity using the manufacturer-supplied correction factors. For all titrations the buffer was 10 mM HEPES and 100 mM NaCl. Titrations were performed in 3 mL of buffer by adding aliquots of the appropriate lanthanide to 50 nM solutions of the appropriate protein to obtain a titration curve. The protein concentration of the stock solutions used in photophysical experiments was determined by UV absorption at 280 nm in a 6 M guanidinium hydrochloride solution using the known extinction coefficient of Trp. After a background data point was recorded, five 1 μL aliquots of 40 μM Tb^{3+} were added, followed by five aliquots of 100 μM Tb^{3+} and three aliquots of 200 μM Tb^{3+}. After each addition, the solution was mixed and a data point taken. All data points represent the average values from three independent titrations. The data were fit using SPECFIT/32, using a 1:1 binding model, which determines log β values, where β is the binding constant. Errors reported for the K_D measurements represent the standard deviation of the results from three independent titrations.

4.3. Determination of Tb^{3+}-Bound Water Molecules. Luminescence lifetimes were measured for all proteins in buffered solutions in a Fluoromax-3 (Jobin Yvon Horiba) spectrometer, equipped with a Spex 1934D3 phosphorimeter. The intensity at 544 nm (Tb^{3+}) was monitored at 60 μs increments for 12 ms after an initial delay of 50 μs, following a lamp pulse at 280 nm from a xenon flash lamp. The reported data are the average of three runs. Using Kaleidagraph, the curves were fit to a monoexponential $[I(t) = I(0)\ e^{(-t/\tau)}]$, where $I(t)$ is the luminescence intensity at time t after the excitation pulse, $I(t)$ is the initial intensity at $t = 0$, and τ is the lifetime. The number of bound water molecules q can be determined by measuring the rate constant of luminescence decay τ^{-1} in pure H_2O and pure D_2O. The value of τ^{-1} for D_2O is determined by measuring the lifetime in varying concentrations of D_2O and H_2O. The value of q can than be calculated using the equation $q = A[(\tau_{H_2O})^{-1} - (\tau_{D_2O})^{-1} - 0.06\ \text{ms}]$, where A is the sensitivity of lanthanide to vibronic quenching, τ is the lifetime in the specified solvent, and 0.06 ms is the correction factor for outer-sphere water molecules.[74]

4.4. NMR Experiments. NMR experiments were performed in buffer containing 10 mM HEPES, 100 mM NaCl, 5 mM β-ME, 10 μM DSS, and 9/1 (v/v) H_2O/D_2O. Samples were prepared by careful titration of a protein solution below 0.1 mM with 10 × 0.11 equiv of lanthanide, either Tb^{3+} or Lu^{3+}. The final sample with 1.1 equiv of lanthanide was concentrated to 0.5 mM using Amicon Centriprep/Centricon centrifugal concentrator devices. All spectra were recorded at 293 K on a Bruker Avance 600 MHz spectrometer equipped with a 5 mm TXI CryoProbe H−C/N−D with a single axis. $^1H-^{15}N$ HSQC spectra were recorded using 2304 × 512 data points in t_2 and t_1, respectively, spectral widths of 14 × 40 ppm in ω_2 and ω_1, and 16 scans per t_1 increment with a z gradient.

RDCs were obtained by subtraction of the scalar $^1J_{H^N}$ coupling of the superposition of scalar and dipolar coupling, both measured in $^1H-^{15}N$ IPAP-HSQCs. They were recorded using 2304 × 1024 data points in t_2 and t_1, respectively, spectral widths of 14 × 40 ppm in ω_2 and ω_1, and 32 scans per t_1 increment with a z gradient at 293 K. Scalar couplings were measured using diamagnetic Lu^{3+}, whereas paramagnetic Tb^{3+} was used for RDC measurements. Deconvolution of the picked peaks was performed in Topspin2.1 using dcon2d.

The 3D $^1H-^{15}N$ NOESY-HSQC experiment was recorded on a Bruker AV600 NMR spectrometer. The mixing time was 150 ms, and the ω_3, ω_2, and ω_1 sweep widths were 8417.5, 1762.9, and 7498.5 Hz (corresponding to 29 ppm in the ^{15}N dimension), respectively.

The bootstrapping procedure was performed using Echidna[83] to assign paramagnetic peaks, and the back-calculation of the experimental PCS as well as the determination of the estimated lanthanide position, $\Delta\chi_{a,r}$ tensor components, and distances of the backbone amide protons to the metal center were performed using the program Numbat.[84]

Back-calculated RDC values and alignment tensors were determined using the program PALES,[79] assuming an order parameter $S = 1$.

^{15}N longitudinal relaxation rates (T_1) were obtained using relaxation delays of 100, 200, 400, 600, 800, 1200, 1600, 2000, and 2800 ms. For measurement of ^{15}N transversal relaxation rates (T_2), delays of 0, 17.6, 35.2, 52.8, 70.4, 105.6, 140.8, 176.0, and 281.6 ms were used. The spectra were recorded at 298 K using 2048 × 160 data points in t_2 and t_1, respectively, spectral widths of 13.3 × 28 ppm in ω_2 and ω_1, and 24 scans per t_1 increment on a Bruker DRX600 spectrometer equipped with a 5 mm TXI RT 1H{$^{13}C/^{15}N$} with a z gradient. The {^1H}−^{15}N HetNOE was measured interleaved, using 2048 × (2 × 128) data points, spectral widths of 13.3 × 21.7 ppm, and 64 scans per t_1 increment on a Bruker DRX600 spectrometer with a 5 mm TXI CryoProbe $^1H\{^{13}C/^{15}N\}$ with z gradient.

4.5. Crystallization and Data Collection of IL1β-S1. For crystallization, proteins were loaded with $TbCl_3$ following a previously established protocol.[5] Briefly, protein was diluted to 1 mg/mL in storage buffer, sodium acetate was added to 10 mM, and terbium chloride (in 1 mM HCl) was added in 10 equal aliquots to a final molar ratio of Tb^{3+} to protein of 1.1:1. Protein was concentrated to 30 mg/mL in preparation for crystallization. Initial screening used the Hampton index screen. IL1β-S1 crystallized readily from 100 mM sodium acetate trihydrate,

Table 2. Data Collection, Structure Determination, and Refinement Statistics of IL1β-S1

Data Collection	
space group and unit cell params	$P6_322$, $a = b = 120.6$ Å, $c = 74.9$ Å
wavelength (Å)	0.95000
resolution limits (Å)	50−2.10 (2.18−2.10)
(highest resolution shell)	
no. of reflns	
measured	294259
unique	19092
completeness (%)	
all data (highest resolution shell)	99.0
R_{sym} (on I) (highest resolution shell)	0.075 (0.274)
$I/\sigma(I)$	
all data (highest resolution shell)	21.2 (3.9)
Structure Determination	
$\langle m \rangle_{SOLVE}$	0.25
$\langle m \rangle_{RESOLVE}$	0.64
Refinement	
resolution (Å)	50−2.1
R factor	0.192
R free	0.224
no. of reflns in test set	3225
no. of non-hydrogen atoms	1486
rms deviations	
bond lengths (Å)	0.008
angles (deg)	1.16
average B factor (Å^2) (all atoms)	31.0

$R_{sym} = \sum|I_{obsd} - \langle I \rangle|/\sum I_{obsd}$.

pH 4.5, 3.0 M NaCl, and the conditions did not require further optimization. Crystals were not obtained for IL1β-S2 and IL1β-S3.

Data were collected at beamline X12C at the National Synchrotron Light Source. IL1β-S1 crystals were cryoprotected by soaking the crystals in 15% glucose in mother liquid and then transferred to 30% glucose solution plus mother liquor. Crystals were flash frozen in the gaseous cryogenic N_2 stream. Data were collected at a wavelength of 0.95 Å and processed with DENZO/SCALEPACK.[91] Crystals diffracted to 2.1 Å and belong to space group $P6(3)22$. Data collection statistics are presented in Table 2.

4.6. X-ray crystal structure solution. The space group assignment was confirmed by systematic absences and the presence of a 20σ peak on the Harker section of the anomalous Patterson map calculated to 2.1 Å. At the wavelength of data collection, $f' \approx -0.45e^-$ and $f'' \approx 6.8e^-$; phases were determined by the program Phenix[92] (FOM 0.49) followed by phase improvement and automatic building (final FOM 0.70), resulting in 83.6% of the backbone being built in an automated fashion including most of the LBT. Protein rebuilding was in COOT,[93] and refinement was carried out in Phenix[92] using phase recombination with the starting phases determined from Tb. The final model contains the entire IL1β molecule including the LBT domain with Tb^{3+}, 2 acetate molecules, and 131 waters. Only the first two residues of the construct and the C-terminal residue could not be observed in the electron density map.

■ ASSOCIATED CONTENT

Supporting Information. Protocols for protein expression and purification, protease cleavage, PAGE analysis, receptor-binding assay, number of bound water molecules in the coordination sphere of terbium, NMR spectra, PCSs, RDC analysis, relaxation data, and complete refs 63 and 92. This material is available free of charge via the Internet at http://pubs.acs.org.

■ AUTHOR INFORMATION

Corresponding Authors

schwalbe@nmr.uni-frankfurt.de; imper@mit.edu; drkallen@bu.edu

■ ACKNOWLEDGMENT

H.S. is a member of the DFG-funded Cluster of Excellence: Macromolecular Complexes. This work was supported by NSF Grant MCB 0744415 to K.N.A. and B.I. A.M.R. acknowledges the NIH for a Ruth L. Kirschstein National Research Service Award. The work was further supported by the EU-funded SPINE2 project. Data for this study were measured at beamline X12C of the National Synchrotron Light Source. Financial support comes principally from the Offices of Biological and Environmental Research and of Basic Energy Sciences of the U.S. Department of Energy and from the National Center for Research Resources of the National Institutes of Health. NMR data were obtained at the Center for Biomolecular Magnetic Resonance (BMRZ) supported by the state of Hesse.

■ REFERENCES

(1) Pazos, E.; Vazquez, O.; Mascarenas, J. L.; Vazquez, M. E. *Chem. Soc. Rev.* **2009,** *38,* 3348–3359.
(2) Marks, K. M.; Nolan, G. P. *Nat. Methods* **2006,** *3,* 591–596.
(3) Allen, K. N.; Imperiali, B. *Curr. Opin. Chem. Biol.* **2010,** *14,* 247–254.
(4) Su, X.-C.; Otting, G. *J. Biomol. NMR* **2010,** 46.
(5) Silvaggi, N. R.; Martin, L. J.; Schwalbe, H.; Imperiali, B.; Allen, K. N. *J. Am. Chem. Soc.* **2007,** *129,* 7114.
(6) Bünzli, J.-C. G. *Acc. Chem. Res.* **2006,** 37.
(7) Richardson, F. S. *Chem. Rev.* **2002,** *82,* 541–552.
(8) Bünzli, J.-C. G.; Piguet, C. *Chem. Soc. Rev.* **2005,** *34,* 1048–1077.
(9) Selvin, P. R. *Annu. Rev. Biophys. Biomol. Struct.* **2002,** *31,* 275–302.
(10) Sandtner, W.; Bezanilla, F.; Correa, A. M. *Biophys. J.* **2007,** *93,* L45–L47.
(11) Sculimbrene, B. R.; Imperiali, B. *J. Am. Chem. Soc.* **2006,** *128,* 7346.
(12) Weis, W. I.; Kahn, R.; Fourme, R.; Drickamer, K.; Hendrickson, W. A. *Science* **1991,** *254,* 1608–1615.
(13) Molina, R.; Stelter, M.; Kahn, R.; Hermoso, J. A. *Acta Crystallogr., Sect. D* **2009,** *65,* 823–831.
(14) Ku, S.-Y.; Smith, G. D.; Howell, P. L. *Acta Crystallogr., Sect. D* **2007,** *63,* 493–499.
(15) Girard, E.; Stelter, M.; Vicat, J.; Kahn, R. *Acta Crystallogr., Sect. D* **2003,** *59,* 1914–1922.
(16) Feeney, J.; Birdsall, B.; Bradbury, A. F.; Biekofsky, R. R.; Bayley, P. M. *J. Biomol. NMR* **2001,** *21,* 41–48.
(17) Gaponenko, V.; Altieri, A. S.; Li, J.; Byrd, R. A. *J. Biomol. NMR* **2002,** *24,* 143–148.
(18) Wöhnert, J.; Franz, K. J.; Nitz, M.; Imperiali, B.; Schwalbe, H. *J. Am. Chem. Soc.* **2003,** *125,* 13338.
(19) Ikegami, T.; Verdier, L.; Sakhaii, P.; Grimme, S.; Pescatore, B.; Saxena, K.; Fiebig, K. M.; Griesinger, C. *J. Biomol. NMR* **2004,** *29,* 339–349.
(20) Boisbouvier, J.; Gans, P.; Blackledge, M.; Brutscher, B.; Marion, D. *J. Am. Chem. Soc.* **1999,** *121,* 7700–7701.
(21) Pintacuda, G.; Hohenthanner, K.; Otting, G.; Müller, N. *J. Biomol. NMR* **2003,** *27,* 115–132.
(22) Iwahara, J.; Schwieters, C. D.; Clore, G. M. *J. Am. Chem. Soc.* **2004,** *126,* 5879–5896.

(23) Donaldson, L. W.; Skrynnikov, N. R.; Choy, W.-Y.; Muhandiram, D. R.; Sarkar, B.; Forman-Kay, J. D.; Kay, L. E. *J. Am. Chem. Soc.* **2001,** *123,* 9843–9847.
(24) Bertini, I.; Cavallaro, G.; Cosenza, M.; Kümmerle, R.; Luchinat, C.; Piccioli, M.; Poggi, L. *J. Biomol. NMR* **2002,** *23,* 115–125.
(25) Blackledge, M. *Prog. NMR Spectrosc.* **2005,** *46,* 23–61.
(26) Pintacuda, G.; Park, A. Y.; Keniry, M. A.; Dixon, N. E.; Otting, G. *J. Am. Chem. Soc.* **2006,** *128,* 3696–3702.
(27) John, M.; Pintacuda, G.; Park, A. Y.; Dixon, N. E.; Otting, G. *J. Am. Chem. Soc.* **2006,** *128,* 12910–12916.
(28) Pintacuda, G.; John, M.; Su, X. C.; Otting, G. *Acc. Chem. Res.* **2007,** *40,* 206.
(29) Saio, T.; Yokochi, M.; Kumeta, H.; Inagaki, F. *J. Biomol. NMR* **2010,** *46,* 271–280.
(30) Tjandra, N.; Bax, A. *Science* **1997,** *278,* 1111–1114.
(31) Tycko, R.; Blanco, F. J.; Ishii, Y. *J. Am. Chem. Soc.* **2000,** *122,* 9340–9341.
(32) Clore, G. M.; Starich, M. R.; Gronenborn, A. M. *J. Am. Chem. Soc.* **1998,** *120,* 10571–10572.
(33) Bertini, I.; Gupta, Y. K.; Luchinat, C.; Parigi, G.; Peana, M.; Sgheri, L.; Yuan, J. *J. Am. Chem. Soc.* **2007,** *129,* 12786–12794.
(34) Dethoff, E. A.; Hansen, A. L.; Zhang, Q.; Al-Hashimi, H. M. *J. Magn. Reson.* **2009,** *202,* 117–121.
(35) Lee, L.; Sykes, B. D. *Biochemistry* **1981,** *20,* 1156–1162.
(36) Tolman, J. R.; Flanagan, J. M.; Kennedy, M. A.; Prestegard, J. H. *Proc. Natl. Acad. Sci. U.S.A.* **1995,** *92,* 9279–9283.
(37) Allegrozzi, M.; Bertini, I.; Janik, M. B. L.; Lee, Y.-M.; Liu, G.; Luchinat, C. *J. Am. Chem. Soc.* **2000,** *122,* 4154–4161.
(38) Bertini, I.; Gelis, I.; Katsaros, N.; Luchinat, C.; Provenzani, A. *Biochemistry* **2003,** *42,* 8011–8021.
(39) Gaponenko, V.; Dvoretsky, A.; Walsby, C.; Hoffman, B. M.; Rosevear, P. R. *Biochemistry* **2000,** *39,* 15217–15224.
(40) Ma, C.; Opella, S. J. *J. Magn. Reson.* **2000,** *146,* 381–384.
(41) Tuechelmann, A.; Schwalbe, H.; Griesinger, C. Presented at the 3rd European Conference, Oxford, U.K., 1998.
(42) Franklin, S. J.; Raymond, K. N. *Inorg. Chem.* **2002,** *33,* 5794–5804.
(43) Gaponenko, V.; Sarma, S. P.; Altieri, A. S.; Horita, D. A.; Li, J.; Byrd, R. A. *J. Biomol. NMR* **2004,** *28,* 205–212.
(44) Haberz, P.; Rodriguez-Castaneda, F.; Junker, J.; Becker, S.; Leonov, A.; Griesinger, C. *Org. Lett.* **2006,** *8,* 1275–1278.
(45) Pintacuda, G.; Moshref, A.; Leonchiks, A.; Sharipo, A.; Otting, G. *J. Biomol. NMR* **2004,** *29,* 351–361.
(46) Häussinger, D.; Huang, J.-r.; Grzesiek, S. *J. Am. Chem. Soc.* **2009,** *131,* 14761–14767.
(47) Prudêncio, M.; Rohovec, J.; Peters, J. A.; Tocheva, E.; Boulanger, M. J.; Murphy, M. E. P.; Hupkes, H.-J.; Kosters, W.; Impagliazzo, A.; Ubbink, M. *Chem.—Eur. J.* **2004,** *10,* 3252–3260.
(48) Keizers, P. H. J.; Saragliadis, A.; Hiruma, Y.; Overhand, M.; Ubbink, M. *J. Am. Chem. Soc.* **2008,** *130,* 14802–14812.
(49) Keizers, P. H. J.; Desreux, J. F.; Overhand, M.; Ubbink, M. *J. Am. Chem. Soc.* **2007,** *129,* 9292–9293.
(50) Su, X.-C.; Man, B.; Beeren, S.; Liang, H.; Simonsen, S.; Schmitz, C.; Huber, T.; Messerle, B. A.; Otting, G. *J. Am. Chem. Soc.* **2008,** *130,* 10486–10487.
(51) Brittain, H. G.; Richardson, F. S.; Martin, R. B. *J. Am. Chem. Soc.* **1976,** *98,* 8255–8260.
(52) MacManus, J. P.; Hogue, C. W.; Marsden, B. J.; Sikorska, M.; Szabo, A. G. *J. Biol. Chem.* **1990,** *265,* 10358–10366.
(53) Franz, K. J.; Nitz, M.; Imperiali, B. *ChemBioChem* **2003,** *4,* 265–271.
(54) Nitz, M.; Franz, K. J.; Maglathlin, R. L.; Imperiali, B. *ChemBioChem* **2003,** *4,* 272–276.
(55) Nitz, M.; Sherawat, M.; Franz, K. J.; Peisach, E.; Allen, K. N.; Imperiali, B. *Angew. Chem., Int. Ed.* **2004,** *43,* 3682–3685.
(56) Martin, L. J.; Sculimbrene, B. R.; Nitz, M.; Imperiali, B. *QSAR Comb. Sci.* **2005,** *24,* 1149.
(57) Zhuang, T.; Lee, H.-S.; Imperiali, B.; Prestegard, J. H. *Protein Sci.* **2008,** *17,* 1220–1231.
(58) Su, X.-C.; Huber, T.; Dixon, N. E.; Otting, G. *ChemBioChem* **2006,** *7,* 1599–1604.
(59) Su, X.-C.; McAndrew, K.; Huber, T.; Otting, G. *J. Am. Chem. Soc.* **2008,** *130,* 1681–1687.
(60) Saio, T.; Ogura, K.; Yokochi, M.; Kobashigawa, Y.; Inagaki, F. *J. Biomol. NMR* **2009,** *44,* 157–166.
(61) Martin, L. J.; Hähnke, M. J.; Nitz, M.; Wohnert, J.; Silvaggi, N. R.; Allen, K. N.; Schwalbe, H.; Imperiali, B. *J. Am. Chem. Soc.* **2007,** *129,* 7106–7113.
(62) Zheng, C.; Kurgan, L. *BMC Bioinf.* **2008,** *9,* 430.
(63) Schwede, T.; et al. *Structure* **2009,** *17,* 151–159.
(64) Vigers, G. P. A.; Anderson, L. J.; Caffes, P.; Brandhuber, B. J. *Nature* **1997,** *386,* 190–194.
(65) Clore, G. M.; Wingfield, P. T.; Gronenborn, A. M. *Biochemistry* **1991,** *30,* 2315–2323.
(66) Arico-Muendel, C. C.; Patera, A.; Pochapsky, T. C.; Kuti, M.; Wolfson, A. J. *Protein Eng.* **1999,** *12,* 189–202.
(67) Wolfson, A. J.; Kanaoka, M.; Lau, F.; Ringe, D.; Young, P.; Lee, J.; Blumenthal, J. *Biochemistry* **1993,** *32,* 5327–5331.
(68) Casadio, R.; Frigimelica, E.; Boss, P.; Neumann, D.; Martin, M. U.; Tagliabue, A.; Boraschi, D. *FEBS Lett.* **2001,** *499,* 65–68.
(69) Wingfield, P.; Graber, P.; Alan, R. S.; Alan, R.; Gronenborn, A. M.; Clore, M. G.; MacDonald, R. H. *Eur. J. Biochem.* **1989,** *179,* 565–571.
(70) Studier, F. W. *Protein Expression Purif.* **2005,** *41,* 207–234.
(71) Dinarello, C. A. *Blood* **1996,** *87,* 2095–2147.
(72) Martin, M. U.; Falk, W. *Eur. Cytokine Network* **1997,** *8,* 5–17.
(73) Horrocks, W. D.; Sudnick, D. R. *J. Am. Chem. Soc.* **2002,** *101,* 334–340.
(74) Beeby, A.; Clarkson, I. M.; Dickins, R. S.; Faulkner, S.; Parker, D.; Royle, L.; de Sousa, A. S.; Williams, J. A. G.; Woods, M. *J. Chem. Soc., Perkin Trans. 2* **1999,** 493–503.
(75) Bleaney, B. *J. Magn. Reson.* **1972,** *8,* 91–100.
(76) Bertini, I.; Luchinat, C.; Parigi, G. *Prog. NMR Spectrosc.* **2002,** *40,* 249–273.
(77) Otting, G. *J. Biomol. NMR* **2008,** *42,* 1–9.
(78) Clore, G. M.; Gronenborn, A. M.; Bax, A. *J. Magn. Reson.* **1998,** *133,* 216–221.
(79) Zweckstetter, M. *Nat. Protoc.* **2008,** *3,* 679–690.
(80) Rule, G. S.; Hitchens, T. K. *Fundamentals of Protein NMR Spectroscopy*; Springer: Dordrecht, The Netherlands, 2006.
(81) Bryce, D. L.; Bax, A. *J. Biomol. NMR* **2004,** *28,* 273–287.
(82) Driscoll, P. C.; Clore, G. M.; Marion, D.; Wingfield, P. T.; Gronenborn, A. M. *Biochemistry* **1990,** *29,* 3542–3556.
(83) Schmitz, C.; John, M.; Park, A. Y.; Dixon, N.; Otting, G.; Pintacuda, G.; Huber, T. *J. Biomol. NMR* **2006,** *35,* 79–87.
(84) Schmitz, C.; Stanton-Cook, M.; Su, X.-C.; Otting, G.; Huber, T. *J. Biomol. NMR* **2008,** *41,* 179–189.
(85) Bertini, I.; Janik, M. B. L.; Lee, Y.-M.; Luchinat, C.; Rosato, A. *J. Am. Chem. Soc.* **2001,** *123,* 4181–4188.
(86) Bertini, I.; Del Bianco, C.; Gelis, I.; Katsaros, N.; Luchinat, C.; Parigi, G.; Peana, M.; Provenzani, A.; Zoroddu, M. A. *Proc. Natl. Acad. Sci. U.S.A.* **2004,** *101,* 6841–6846.
(87) Brünger, A. T.; Adams, P. D.; Clore, G. M.; DeLano, W. L.; Gros, P.; Grosse-Kunstleve, R. W.; Jiang, J.-S.; Kuszewski, J.; Nilges, M.; Pannu, N. S.; Read, R. J.; Rice, L. M.; Simonson, T.; Warren, G. L. *Acta Crystallogr., Sect. D: Biol. Crystallogr.* **1998,** *54,* 905–921.
(88) Lipari, G.; Szabo, A. *J. Am. Chem. Soc.* **1982,** *104,* 4546–4559.
(89) Lipari, G.; Szabo, A. *J. Am. Chem. Soc.* **1982,** *104,* 4559–4570.
(90) Dosset, P.; Hus, J. C.; Blackledge, M.; Marion, D. *J. Biomol. NMR* **2000,** *16,* 23.
(91) Otwinowski, Z.; Minor, W.; Carter, C. W. J. *Methods Enzymol.* **1997,** *276,* 307–326.
(92) Adams, P. D; et al. *Acta Crystallogr., Sect. D: Biol. Crystallogr.* **2009,** *66,* 213–221.
(93) Emsley, P.; Cowtan, K. *Acta Crystallogr., Sect. D: Biol. Crystallogr.* **2004,** *60,* 2126–2132.